Applied Catalysis A: General 498 (2015) 230–240

Contents lists available at ScienceDirect

Applied Catalysis A: General

journal homepage: www.elsevier.com/locate/apcata

Cobalt-incorporated, nitrogen-doped carbon nanofibers as effective non-precious catalyst for methanol electrooxidation in alkaline medium

Badr M. Thamer[a], Mohamed H. El-Newehy[a,b,**], Salem S. Al-Deyab[a], Mohammad Ali Abdelkareem[d], Hak Yong Kim[c], Nasser A.M. Barakat[c,d,*]

[a] Petrochemical Research Chair, Department of Chemistry, College of Science, King Saud University, Riyadh 11451, Saudi Arabia
[b] Department of Chemistry, Faculty of Science, Tanta University, Tanta 31527, Egypt
[c] Organic Materials and Fiber Engineering Department, College of Engineering, Chonbuk National University, Jeonju, South Korea
[d] Minia University, Faculty of Engineering, Chemical Engineering Department, El Minia, Egypt

ARTICLE INFO

Article history:
Received 24 November 2014
Received in revised form 11 March 2015
Accepted 26 March 2015
Available online 2 April 2015

Keywords:
Electrospinning
Methanol oxidation
Fuel cells
Nitrogen-doping
Cobalt

ABSTRACT

Among the nanosupports, carbon nanofibers distinctly enhance the performance of the functional electrocatalysts because the adsorption capacity and low resistance electron transfer due to the large axial ratio. Moreover, nitrogen doping shows positive influence toward electrooxidation ability. In this study, Co-incorporated and nitrogen-doped carbon nanofibers are introduced as effective non-precious electrocatalyst for methanol oxidation in the alkaline medium. The introduced NFs have been prepared using facile, simple, high yield, low cost, and effective technique; electrospinning. Typically, calcination of cobalt acetate/urea/poly(vinyl alcohol) electrospun mats at 850 °C in argon atmosphere leads to produce the introduced nanofibers. The structure, composition and morphology were characterized by FT-IR, XRD, EDX, FE-SEM and TEM techniques. The electrocatalytic activity of the introduced nanofibers toward methanol oxidation was evaluated by cyclic voltammetry (CV). Study the influence of the nitrogen content could be investigated by adjusting the urea content in the original electrospun nanofiber mats. The results indicated that the activity of the catalyst increases with increasing urea content in the electrospun solution up to 4%. A maximum current density was 100.84 mA cm^{-2} for Co/N(4%)-CNFs that was higher than the undoped ones (63.56 mA cm^{-2}). Moreover, good chemical stability was observed due to covering the metals NPs by carbon shells. Overall, nitrogen doping enhances electrocatalytic activity of Co/CNFs toward methanol oxidation in alkaline media.

1. Introduction

Development a future energy system from sustainable energy sources as an alternative for fossil fuels is considered a key objective of modern research. Direct methanol fuel cells (DMFCs) are the most promising sustainable energy devices because methanol is an inexpensive, readily available, and easily stored and transported liquid fuel [1,2]. Unfortunately, high production cost due to utilizing precious metals electrodes (e.g. Pt) is facing wide commercial application for not only DMFCs but also all the other fuel cells. Accordingly, more efforts are being done to develop low cost materials having good chemical stability and high catalytic activity to replace platinum [3–5]. In the DMFCs, methanol is oxidized to carbon dioxide at the anode according to the reaction: $CH_3OH + H_2O = CO_2 + 6H^+ + 6e$. The reaction is considered to be a combination of adsorption and electrochemical reaction on the anode surface [6,7]. Accordingly, because of the adsorption capacity of carbon, the later has been incorporated in many recently reported electrocatalytic materials, not only for the DMFCs but also other kinds of fuel cells [8–12]. Among the utilized carbon nanostructural supports, the large axial ratio provides the carbon nanofibers additional feature due to the low electron transfer compared to other structures [13,14].

Transition metals nanostructures and their alloys have been studied as an electroactive material for methanol oxidation and

* Corresponding author at: Organic Materials and Fiber Engineering Department, College of Engineering, Chonbuk National University, Jeonju, South Korea. Tel.: +82 63 2702363; fax: +82 63 270 4248.
** Corresponding author at: Petrochemical Research Chair, Department of Chemistry, College of Science, King Saud University, Riyadh 11451, Saudi Arabia. Tel.: +966 14675899; fax: +966 14676992.
E-mail addresses: melnewehy@ksu.edu.sa (M.H. El-Newehy), nasser@jbnu.ac.kr (N.A.M. Barakat).

http://dx.doi.org/10.1016/j.apcata.2015.03.042
0926-860X/

potentially cheaper than platinum [15–18]. However, the high chemical activity is a forcible constraint facing wide utilizing of this new class of materials. Among the utilized transition metals, cobalt gained the lowest attention due to the low electrocatalytic activity of the pristine cobalt. Instead, it is used as a co-catalyst to annihilate the Pt poisoning. Pt–Co alloys have been found to be excellent CO-tolerant catalysts [19]. However, some recent reports have introduced cobalt as a main catalyst [13,20,21]. Compared to nanoparticulate morphology, nanofibers do have low specific surface area which can be considered as negative characteristic in catalytic applications however the large axial ratio proved that it has distinct positive impact in the electrocatalytic oxidation of methanol [22,23]. Currently, many studies are focusing on improving the catalytic activity and stability through incorporation of heteroatoms such as nitrogen into the carbon nanostructure supports. Nitrogen-doped carbon nanostructure owns high surface nucleation sites which allows the anchorage and high dispersion of the catalyst nanoparticles on the support surface material that results in high interaction between nitrogen-doped carbonaceous support and the catalytic metals [24–26]. On the other hand, nitrogen doping improves the durability of the resultant carbon-support catalysts because of the enhanced π bonding [27,28], and the basic property [29] due to the strong electron donor behavior of nitrogen. Nitrogen-doped carbon nanotubes/nanofibers (N-CNT/N-CNF) showed enhanced catalytic activity toward oxygen reduction reaction (ORR) [30–32]. Most of the previous studies were used nitrogen doped carbon nanostructure with noble metals or their alloys as catalysts (e.g. Pt, Ru, etc.) for methanol oxidation [33]. Recently, the same authors studied the influence of nitrogen doping on the electrocatalytic activity of nickel-doped carbon nanofibers; the results indicated that nitrogen doping has featured influence [34]. In literature, there are several methods have been introduced to synthesis the nanofibers, however among these reported techniques, electrospinning have drawn the most attention due to several advantages including simplicity, high yield, low cost and easy morphology control [35–38].

In this work, cobalt-decorated and nitrogen-doped carbon nanofibers (Co/N-CNFs) are introduced as anode for methanol oxidation. The introduced catalysts was fabricated by using electrospinning technique and followed by carbonization process at 850 °C. The experimental results revealed good electrocatalytic activity and non-observable influence on the good stability of Co/N-CNFs toward methanol oxidation in alkaline medium especially at high nitrogen content.

2. Experimental

2.1. Materials

Cobalt(II) acetate tetrahydrate ($CoAc{\cdot}H_2O$, 98%), poly(vinyl alcohol) (PVA, MW = 88 K g mol^{-1}), urea (99%), methanol, potassium hydroxide, isopropyl alcohol, Nafion 117 (10 wt%), diamond suspension and acetone were purchased from Sigma–Aldrich Co. Those materials were utilized without any further purification. Distilled water was used as solvent.

2.2. Preparation of N-CoCNFs catalysts

PVA (10%, w/w) solution was prepared at 70 °C with a mechanical stirring for 2 h to obtain clear solution. Cobalt acetate tetrahydrate ($Co(Ac{\cdot}4H_2O)$ aqueous solution (20%, w/w) was prepared by sonication for 15 min at room temperature using ultrasonication. The sol–gel was prepared through mixing PVA and $CoAc{\cdot}4H_2O$ solutions in a weight ratio of 4:1 and then different concentrations of urea (0, 1, 2, 3, 4, 5%, w/w) were added and stirred for 5 h at 50 °C. The viscous gels were electrospun to produce nanofibers mats. The procedure can be summarized as following; the sol–gel of PVA/CoAc or PVA/CoAc/urea was placed in 20 mL plastic syringe attached to the digital hypodermic syringe and fed into the stainless steel needle at a flow rate of 0.9 mL/h, which was maintained by the digital hypodermic syringe pump. A collecting drum was covered with a polyethylene sheet. The applied voltage was 17–20 kV and TCD was 15 cm. The electrospinning process was carried out at room temperature and humidity was $\geq$35%. The collected NFs mats were peeled from surface of polyethylene sheet. The NFs mats were dried for 24 h at 80 °C under vacuum. Later on, the collected nanofibers mats were calcined in an argon atmosphere at 850 °C with a heating rate of 2.83 °C min^{-1} for 5 h. Nanofiber mats were left inside the furnace until cooled to room temperature and evolved argon gas in the reaction medium to prevent oxidation.

2.3. Preparation of working electrode for methanol oxidation

It was carried out by mixing 2 mg of the functional material, 20 μL Nafion 117 (5 wt%) and 420 μL isopropanol. The slurry was sonicated for 30 min at room temperature. A 15 μL from the prepared slurry was poured on the active area of the glassy carbon electrode (0.07 cm^2 area) which was then subjected to drying process at 80 °C for 20 min. Before poured the slurry solution on the glassy carbon electrode, it should be cleaned by acetone and distillated water then polished by adding one drop of diamond suspension to smooth emery paper and moved the glassy carbon electrode on it until became like mirror and then cleaned by acetone and distilled water and again cleaned by acetone and distilled water.

2.4. Characterization

The surface morphology of samples was studied by FESEM (JEOL-JSM-2100F, Japan) equipped. Thermogravimetric analyses (TGA) for the prepared electrospun mats were performed on TA Instruments (Q500 TGA) to study thermal properties of nanofibers mats. The crystallinity and structure of the as-prepared catalyst was studied by X-ray diffractometer (XRD, Bruker D8 DISCOVER), FT-IR (Bruker Optic Tensor 27, Germany), respectively. Normal and high resolution images of prepared catalysts were observed by transmission electron microscope (TEM, JEOL-JEM-2100, Japan). The electrocatalytic activities of prepared catalysts as anode (working electrode) for methanol electro-oxidation were performed by Versa STAT 4 (USA) electrochemical analyzer and a conventional three electrodes electrochemical cell. An Ag/AgCl electrode and Pt wire were used as the reference and auxiliary (counter) electrode, respectively.

3. Results and discussion

3.1. Characterization of Co/N-CNFs catalyst

FESEM instrument was used to study the changes in morphology of fibers caused by addition of urea with different concentration before and after calcination and determine the average diameters of nanofibers. Fig. 1 shows FE-SEM images of the electrospun PVA/CoAc nanofiber mats without and with different concentration of urea before calcination. As shown in this figure, the obtained nanofibers are relatively smooth and the diameter of nanofibers increase with increase the concentration of urea. This may be attributed to the increasing of viscosity of the precursor solution due to the urea interaction with PVA polymer which demonstrated by FT-IR in Fig. 5. Moreover, as shown in Fig. 1, NFs have a random orientation because of the bending instability associated with the

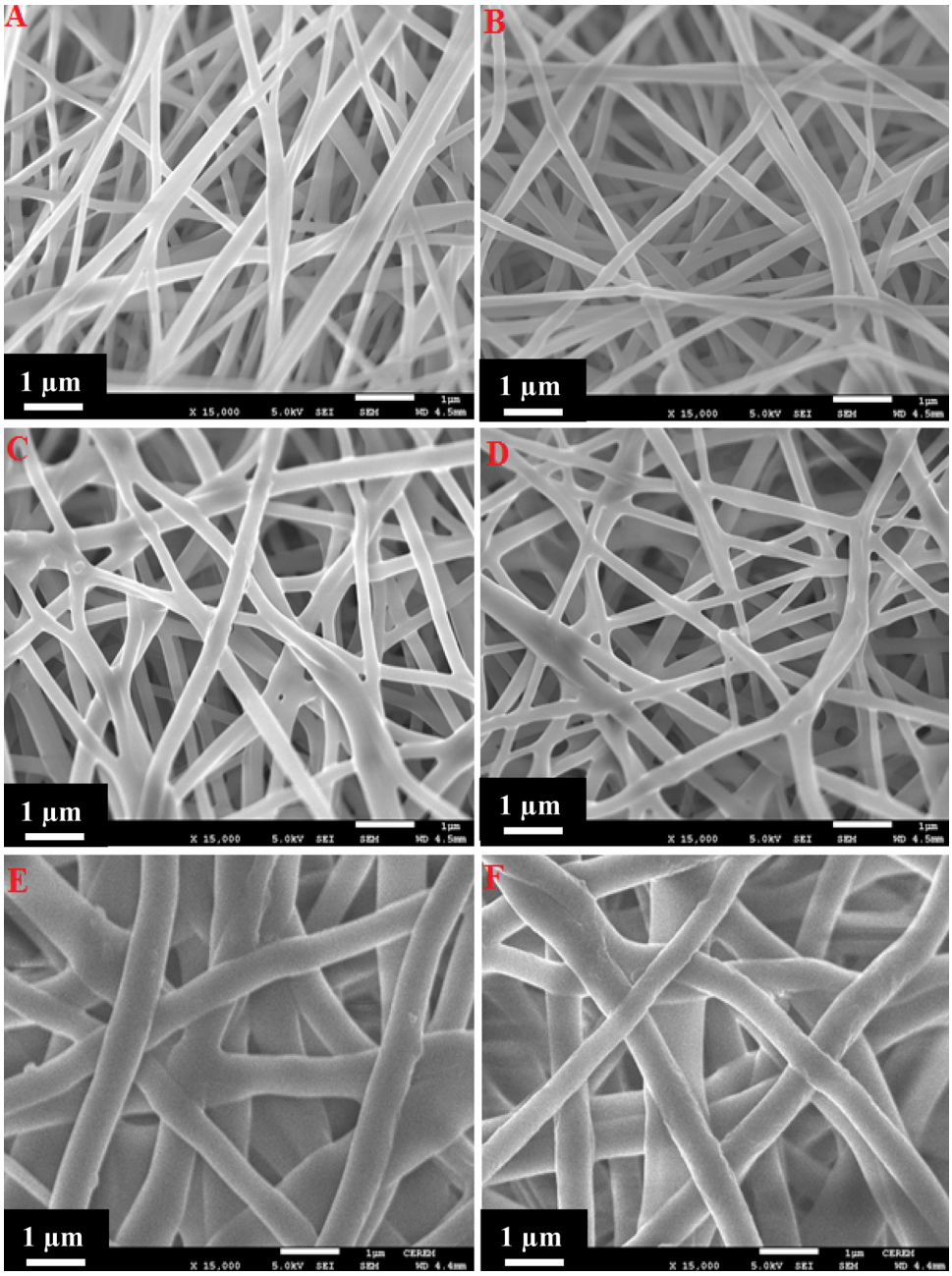

Fig. 1. SEM images for the PVA/CoAc nanofibers mats with different urea content: (A) 0.0%, (B) 1.0%, (C) 2.0%, (D) 3.0%, (E) 4.0%, and (F) 5.0%.

spinning jet. After calcination process, the nanofibrous morphology of nanofibers was slightly changed and the average diameters of the fibers became smaller (Fig. 2). This can be attributed to the low thermal decomposition rate of the polymer upon calcination of the electrospun nanofiber mats in an argon atmosphere which leads to preserving the nanofibrous morphology [39,40].

Fig. 3 displays the effect of urea content in the original electrospun solution on the average diameter of the obtained electrospun nanofibers and the produced ones after the calcination process. As shown, increasing the urea content leads to increase the average diameter which can be attributed, as aforementioned, to increase the viscosity of the electrospun solution with increasing the urea content.

To investigated the structure of the obtained nanofibers and Co NPs size after the calcination process, XRD analysis was carried out. As shown in Fig. 4, the strong diffraction peaks at $2\theta = \sim 44.3^\circ$, 51.6°, 75.9° and 92.2° correspond to the (1 1 1), (2 0 0), (2 2 0) and (3 1 1) planes of the face-centered cubic crystalline cobalt. According to the XRD database, these peaks indicate formation of pristine Co. No other peaks can be observed in the spectra (except graphite peak) which indicate that the sample is free from cobalt oxide or any other crystalline materials.

The average grain size in the formed cobalt nanoparticles can be estimated by Scherrer's equation (Eq. (1)) through analysis of the (1 1 1) cobalt peaks using the calculated full width half max (FWHM).

$$\tau = \frac{k\lambda}{\beta \cos\theta} \quad (1)$$

K is constant (0.9), λ is the X-ray wavelength, β is the full width half maximum (FWHM), θ is the Bragg angle and τ is the mean size of the crystalline domains. In general, the average particles size of cobalt

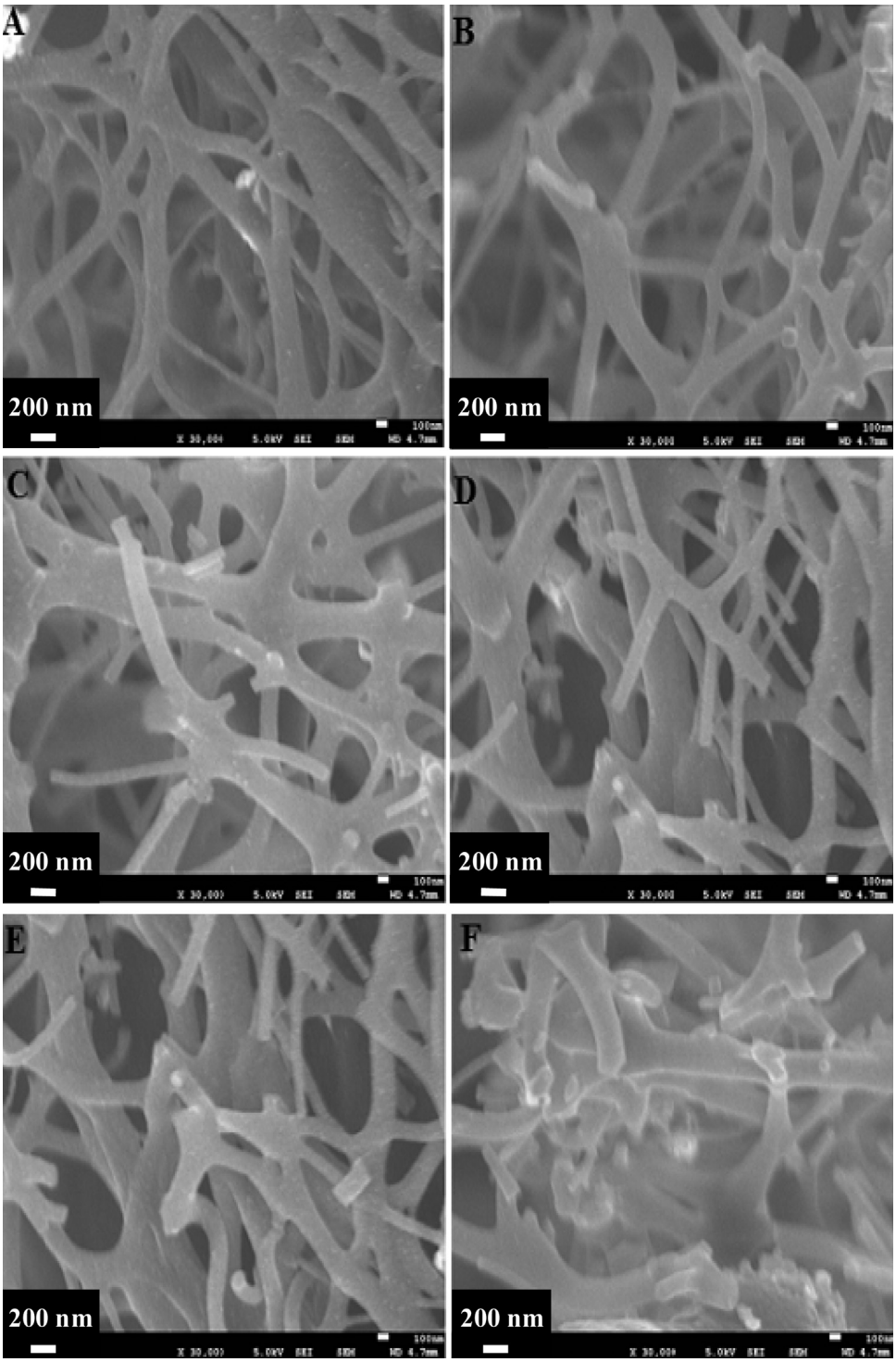

Fig. 2. FE-SEM images of the prepared electrospun mats after calcination in Ar atmosphere at 850 °C: (A) 0.0%, (B) 1.0%, (C) 2.0%, (D) 3.0%, (E) 4.0%, and (F) 5.0% urea.

in Co/N-CNFs was approximately 23 nm. Additionally, the peak at 2θ of 26.3° corresponds to an experimental d spacing of 3.37 Å indicating presence of graphite-like carbon (d (0 0 2), JCPDS; 41-1487). Moreover, the broad peak at 10° for the sample having 4 wt% urea (d spectrum) can be assigned to formation of some sheets from graphene oxide; [0 0 2] crystal plane [41].

It is known that XRD can only investigate the crystalline material so nitrogen cannot be detected in the XRD spectra. EDX is an analytical technique used to determine amount and composition of element in sample. Fig. 5 shows the elemental composition of nitrogen undoped and doped cobalt carbon nanofibers after the calcination process. The results shown in this figure confirmed the doped and undoped of Co/CNFs was free from oxygen. Two and three main components are detected in the Co/CNFs and Co/N-CNFs namely: carbon, cobalt, and nitrogen with a different ratio, respectively. Nitrogen was detected in all samples containing urea and its ratio increases with increasing urea concentration in electrospun solution. The ratio of nitrogen increase with increasing urea concentration in precursors and reached to 6.77%.

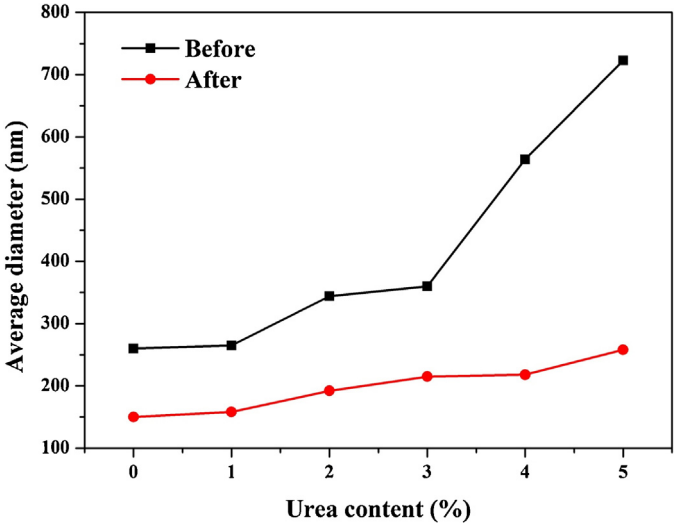

Fig. 3. Influence of the urea content on the average diameter of the electrospun and sintered nanofibers.

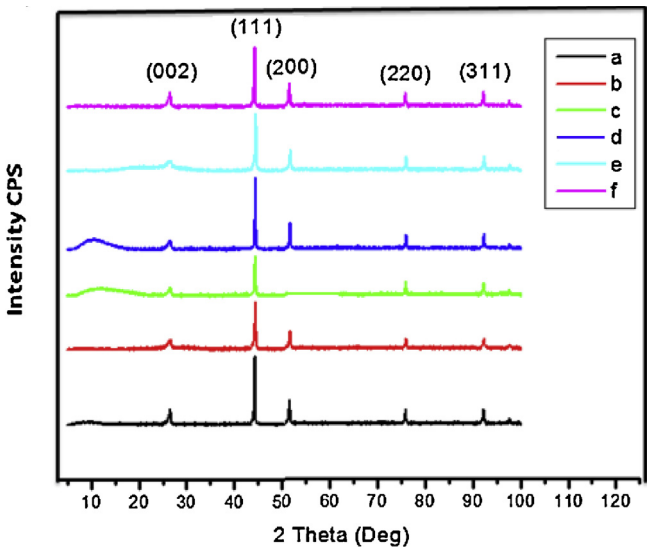

Fig. 4. XRD spectra of Co/CNFs (a) and Co/N-CNFs obtained from electrospun solutions having urea content of 1% (b), 2% (c), 3% (d), 4% (e) and 5% (f).

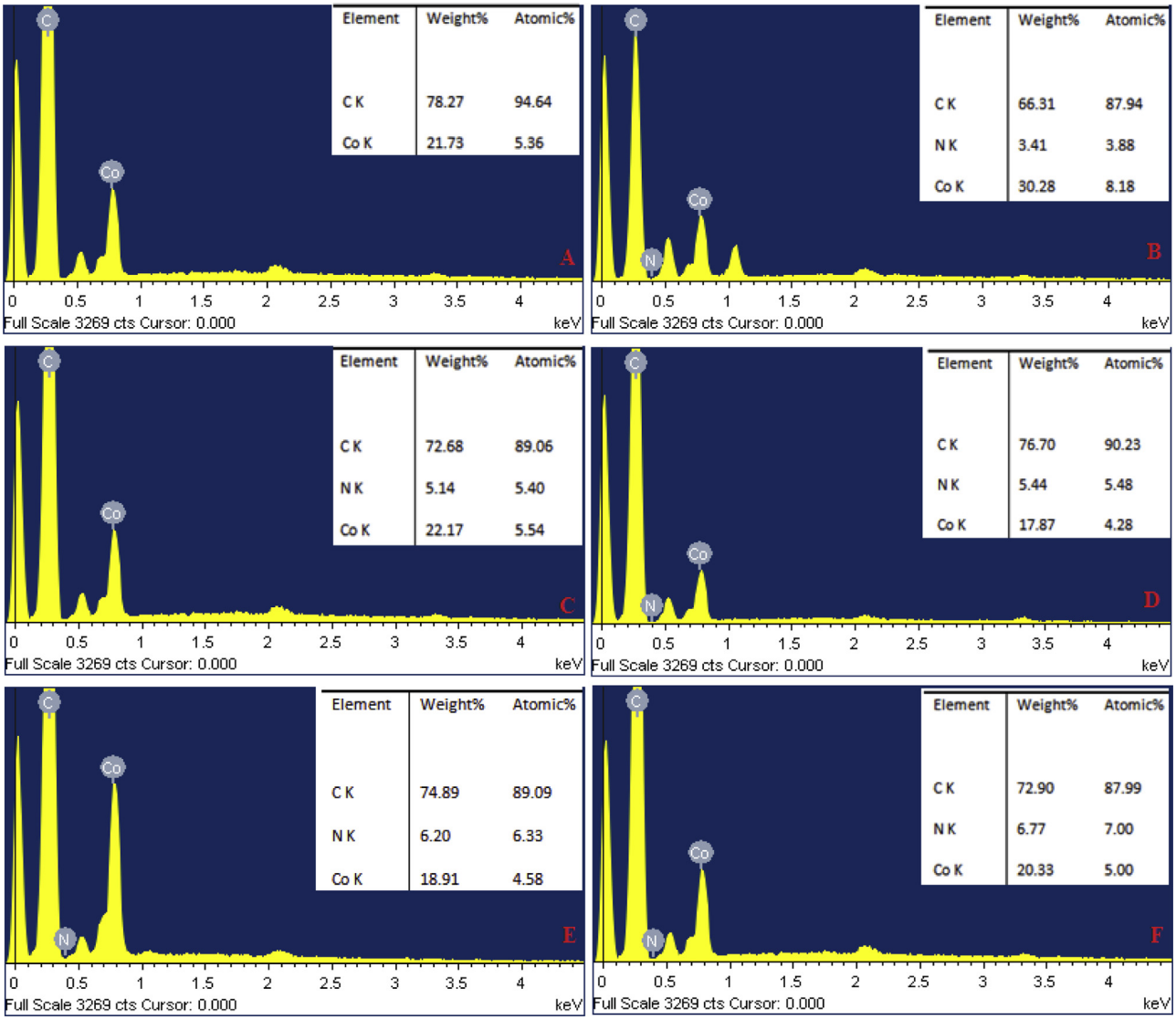

Fig. 5. EDX analyses for Co/CNFs (a) and Co/N-CNFs obtained from electrospun solutions having urea content of 1% (b), 2% (c), 3% (d), 4% (e) and 5% (f).

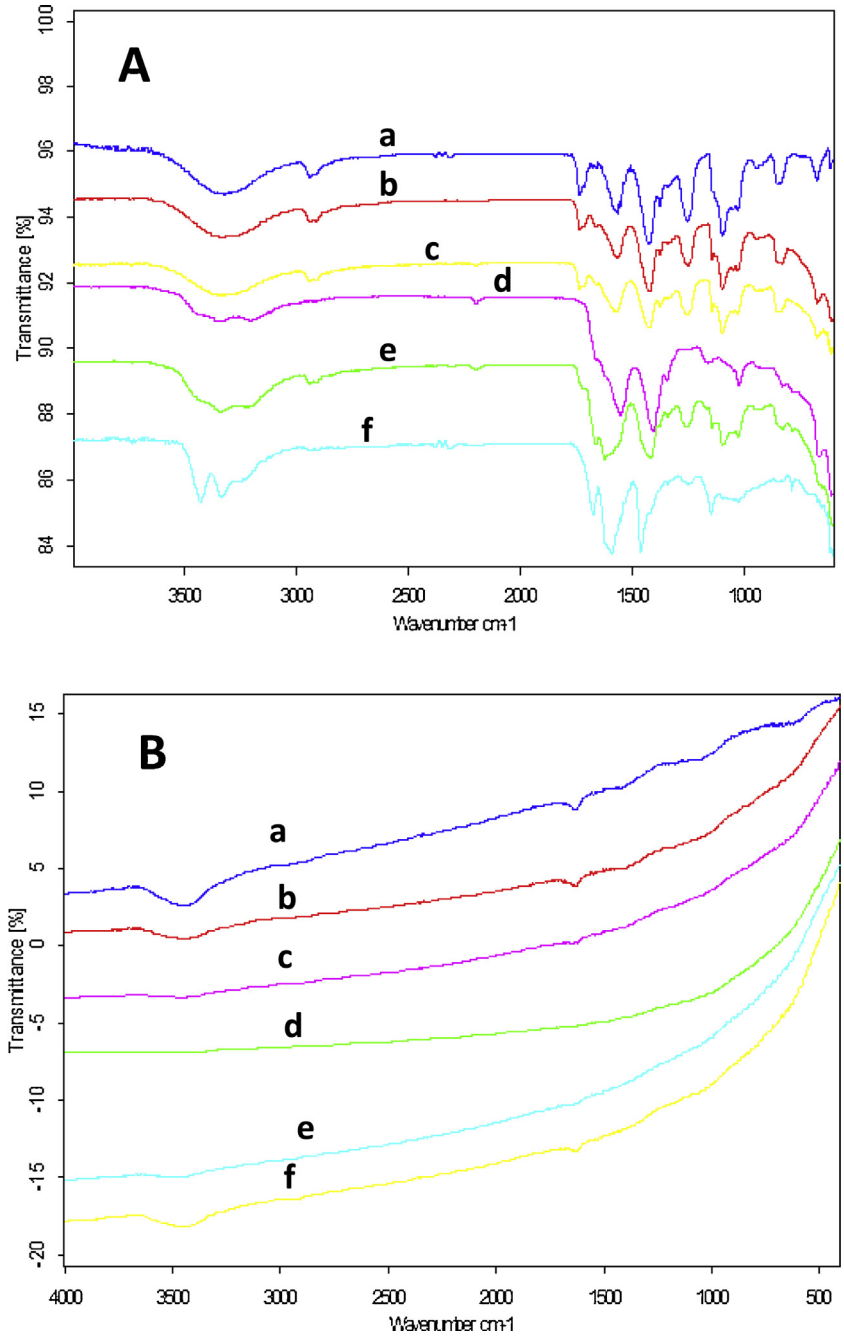

Fig. 6. FT-IR spectra for the prepared nanofibers before (A) and after (B) calcination process: (a) 0%, (b) 1%, (c) 2%, (d) 3%, (e) 4% and (f) 5% urea.

The structure and interaction between the components of the prepared nanofibers were demonstrated by FT-IR. Fig. 6 shows FT-IR spectra of the electrospun nanofibers mats before and after the calcination process. As shown in Fig. 6A the characteristic absorption peaks were observed at ~3325, 2944 and 2910 cm^{-1} due to O—H and C—H symmetric and asymmetric stretching vibration; respectively. Other strong bands at ~1418, 1096, 1045 cm^{-1} correspond to C—H bending, C—O stretching vibration, and the weak band appeared at 1716 cm^{-1} C=O result from acetate group of cobalt acetate and some ester formation in the product [42]. In Fig. 6A spectra b to f, new band can be observed at 2200, 1625 cm^{-1} due to C≡N stretching and N—H bending, respectively. In addition, new single band appeared at ~3435 cm^{-1} due to N—H stretching that indicated the urea interaction with fibers composite and resulted secondary amide group. It is noteworthy mentioning that, the single band at 3435 cm^{-1} appeared obviously when the concentration of urea more than 2% (w/w). Fig. 6B shows the FT-IR spectrum of PVA/CoAc (with and without doping) after calcination. As shown in this figure, the functional groups of PVA and urea disappeared that indicates the degradation of polymer result from sintered at high temperature. However, the observed broad band at 3440 cm^{-1} and weak band at 1630 cm^{-1} can be attributed to stretching and bending vibrations of water molecules [43].

TGA analysis was used to study thermal degradation of electrospun nanofibers under nitrogen atmosphere with heating rate of 10 °C min^{-1}. Fig. 7 shows the TGA with the first derivative of PVA/CoAc and PVA/CoAc/urea (3%) composite. Actually, abnormal decomposition of the acetate anion led to form reducing gases

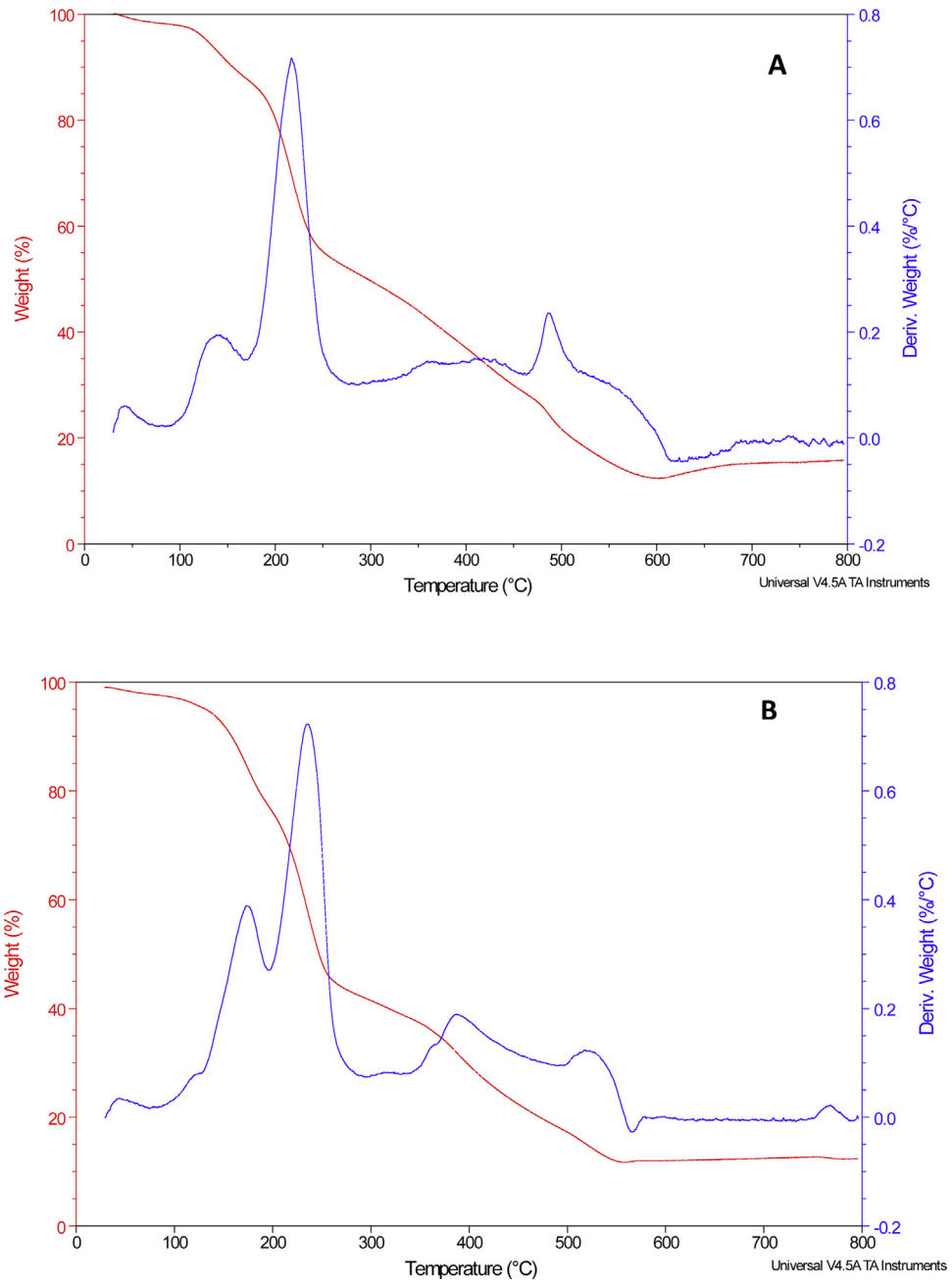

Fig. 7. TGA analyses of PVA/CoAc electrospun nanofibers mats: (A) urea free and (B) urea 3%.

(CO and H_2), these gases are responsible about formation of the pure cobalt. Typically, formation of pure cobalt is conducted according to the following equations [40]:

$$Co(CH_3COO)_2{\cdot}4H_2O \rightarrow Co(OH)(CH_3COO) + 3H_2O + CH_3COOH \quad (2)$$

$$Co(OH)(CH_3COO) \rightarrow 0.5CoO + 0.5CoCO_3 + 0.5H_2O + 0.5CH_3COCH_3 \quad (3)$$

$$CoCO_3 \rightarrow CoO + CO_2 \quad (4)$$

$$CoO + CO \rightarrow Co + CO_2 \quad (5)$$

Degradation of PVA/CoAc achieved in four steps. As shown in Fig. 7 the first and second step at 42–45 °C and 139–175 °C can be assigned to the liberation of physical (moisture) and chemical (combined water molecules with the CoAc) water from the sample, respectively. Second peak appeared at 215 and 237 °C for undoped and doped fibers, respectively can be attributed to degradation of PVA backbone. Considering that the high thermal stability of metal carbonates, the peaks at 361 and 387 °C can be assigned to the decomposition of the synthesized carbonate (Eq. (3)) into monoxide. The formed cobalt monoxide starts to be reduced by carbon monoxide gas which is produced by the decomposition of the acetate at the last peaks at temperatures 487 and 524 °C for undoped and doped fibers [13,39,44,45]. It is noteworthy mentioning that the doping PVA/CoAc electrospun nanofibers by urea reveals more thermal stability than the undoped ones. This may assigned to effect of derivatives of urea during carbonization process that caused partial cross-linked for PVA at initial stage.

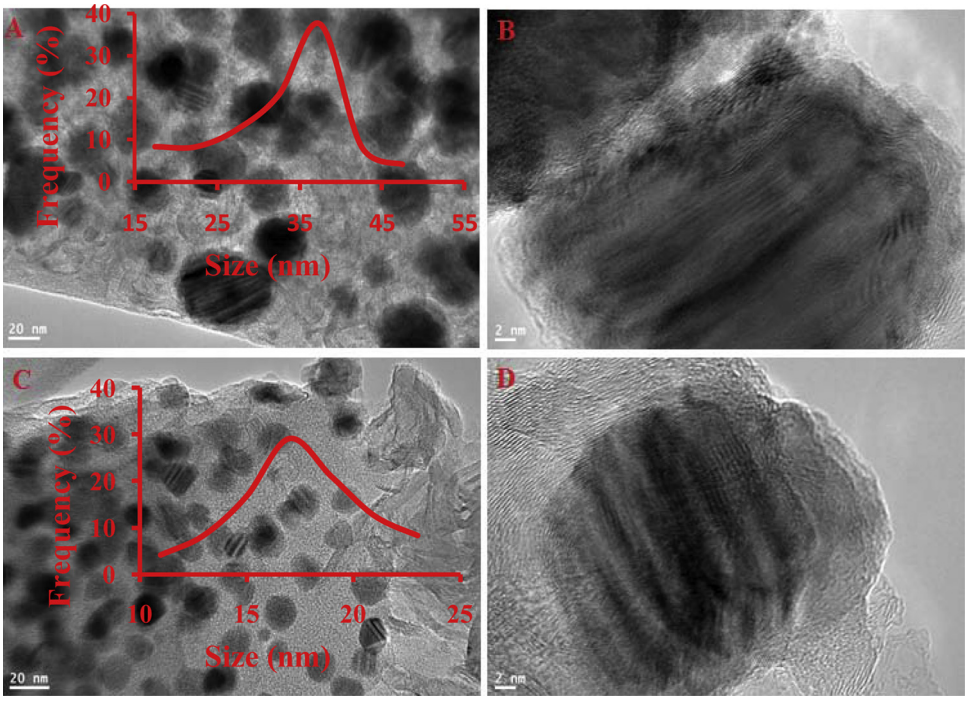

Fig. 8. Low and high magnifications TEM images of the undoped Co/CNFs (A and B) and nitrogen doped-Co/CNFs mats (3%) (C and D) after calcination.

Fig. 8 shows the TEM images of the nitrogen-free and -doped Co/CNFs. A and C images show the obtained powder consist of carbon nanofibers matrix with metallic NPs incorporated. The high magnification HR-TEM images indicate that the presence of parallel atomic planes and appear excellent crystallinity for the graphite layer (Fig. 8B and D). This result confirms FE-SEM result. Moreover, the metallic nanoparticles are enclosed in graphite sheath which can work as protector to save the particles from corrosion during exploiting the introduced nanofibers as electrocatalyst.

The insets in Fig. 8A and C display the particle size distributions for the metallic nanoparticles incorporated in the carbon nanofibers obtained from nitrogen-free and nitrogen-doped (3% urea) Co/CNFs, respectively. As shown, nitrogen doping leads to produce Co/CNFs having smaller size Co nanoparticles (average diameter ~17 nm) compared to the undoped nanofibers (average diameter ~37 nm). Moreover, the doping results in good distribution of the metallic nanoparticles as shown in the images. Beside the metal alkoxides, metal acetates have been widely utilized as metal precursors as these promised salts have good tendency for polycondensation to form with the proper polymers electrospinable sol–gels [44,46–49]. Therefore, the change in the particle size distribution upon nitrogen doping can be attributed to the negative influence of nitrogen on the cobalt acetate polycondensation. In other words, nitrogen doping decreases the polycondensation of the acetate molecules which results in decrease the particle size.

X-ray photoelectron spectroscopy (XPS) can provide the chemical-state information of the detected elements. Fig. 9 displays the obtained XPS results for the nanofibers obtained from electrospun solution having 2 wt% urea. As shown in the figure and the corresponding inset, nitrogen could be detected (N1S at binding energy of 395.4 eV) which confirms the doping of the introduced nanofibers by nitrogen and simultaneously supports the EDX and FTIR results.

3.2. Electrochemistry measurement

Fig. 10 displays the electroactivity of N-doped Co/CNFs (urea content 4%) in 1 M KOH (methanol free) and 5 M methanol in 1 M KOH aqueous solutions. As shown, the introduced electrocatalyst showed a good activity toward methanol oxidation. Interestingly, the oxidation process is observed during the positive potential. Moreover, the onset potential (0.35 mV) for the solution contain methanol is shifted to less value as compared with methanol-free 1 M KOH (0.6 V). Carbon monoxide is an intermediate compound in the methanol electrooxidation, it accumulates on the surface of the electrode till further oxidation step to carbon dioxide. Usually, adsorption of CO appears to take place with the formation of islands of adsorbate [50]; electroactivity appears to be restricted to the outsides of these islands. Accordingly, good catalytic activity is related with the rate of CO removal. Oxidation of the CO leads to appear a peak in the voltammogram at ~550 mV (vs. NHE) [51]. Generally, above 700 mV, the surface is almost free of adsorped CO because of complete oxidation [52]. As shown in the obtained results for

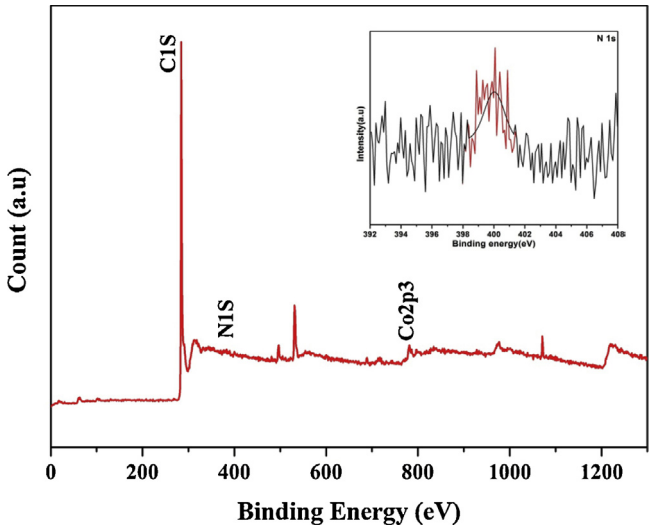

Fig. 9. XPS analysis for the introduced N-doped Co/C NFs obtained from electrospun solution having 2 wt% urea. The inset displays the spectrum at N1S region.

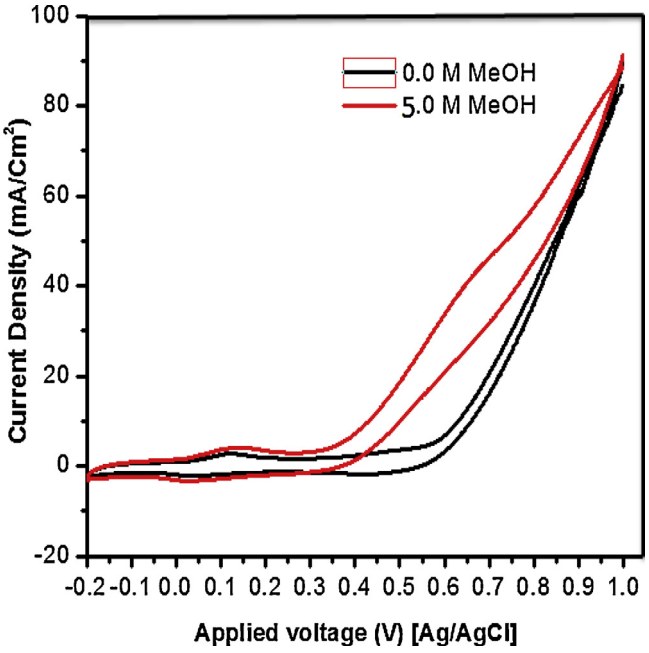

Fig. 10. Consecutive cyclic voltammogram of Co/N-CNFs (urea content 4%) in 1 M KOH at a scan rate of 100 mV s^{-1}.

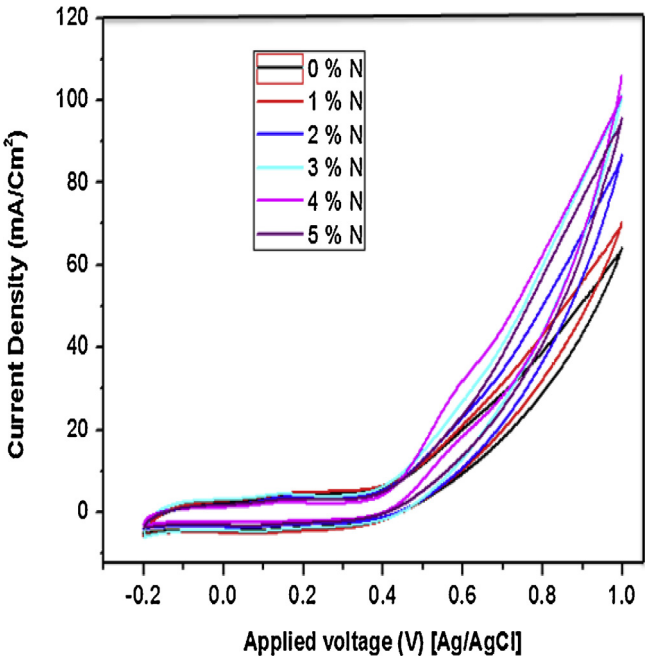

Fig. 11. Study the influence of nitrogen doping on electrocatalytic activity of Co/CNFs toward methanol oxidation at 3 M methanol + 1 M KOH.

the introduced electrocatalyst, the aforementioned CO oxidation peak is not observed which indicates either instant oxidation of CO and/or absence of CO as an intermediate compound. In such a case, the electrooxidation of the methanol on the surface of the introduced catalyst can be explained as carrying out according to this route [52]. Due to polarity of methanol and others intermediates is higher than polarity of CO, the rate adsorption of methanol and other active intermediates on surface catalyst is faster than adsorption of CO. The high adsorption of methanol on surface catalyst is related to presence of nitrogen inside CNFs which increases its polarity and enhances the reactivity of catalyst.

3.2.1. *Influence of nitrogen doping*

The electrocatalytic activity of nitrogen-free cobalt CNFs and N-doped (1, 2, 3, 4 and 5%) cobalt CNFs has been studied by cyclic voltammetry (CV) technique. It was measured at potential range between −0.2 and 1.0 V vs. Ag/AgCl and scans rate 50 mV s^{-1} at 25 °C in 1.0 M KOH and 3.0 M methanol. As shown in Fig. 11, the electrocatalytic activity of nitrogen-containing NFs increased in term of current density. A maximum current density was 100.84 mA cm^{-2} for N (4%)–Co/CNFs which is higher than nitrogen-free cobalt CNFs (63.56 mA cm^{-2}). The observed high performance may be attributed to increasing the conductivity of CNFs and the lone pair electrons in the nitrogen atoms with regard to the conjugated system of a graphite-like hexagonal framework which enhance the electrochemical oxidation of methanol. Moreover, the nitrogen doping in the graphite frameworks could improve the wettability of the interface electrode/electrolyte [53].

3.2.2. *Optimum methanol concentration*

One of the objectives of methanol cells is reducing the volume of fuel by increasing the concentration of methanol but it influences on catalytic activity of the catalyst through decrease of current density. Sample content 4% urea was selected to study the effect of methanol concentration on the electrocatalytic activity because it showed a best catalytic activity toward methanol oxidation as compared to other samples. Fig. 12 displays the anode polarization at different methanol concentration at a scan rate of 50 mV s^{-1} and applied cell potentials ranging from −0.2 to 1.0 V. As shown in Fig. 12 and the corresponding inset which displays the relationship between the methanol concentration and the current density at the anodic peak, the current density increases with increase the methanol concentration up to 2.0 M. Later on, more increase in the methanol concentration leads to sharply decreasing in current density.

3.2.3. *Influence of the scan rate*

The effect of scan rate on the behavior of methanol oxidation at N (4%)–Co/CNFs was investigated at various scan rate (10, 50, 100, 150, 200, 300, 400, 500, 700, 1000 mV s^{-1}) and in 3.0 M methanol as shown in Fig. 13. It can be clearly seen that a peak potential appears at the low scan rate (10 mV s^{-1}; the red arrow) and shifts positively with the increase in the scan rate. This peak can be assigned to CO

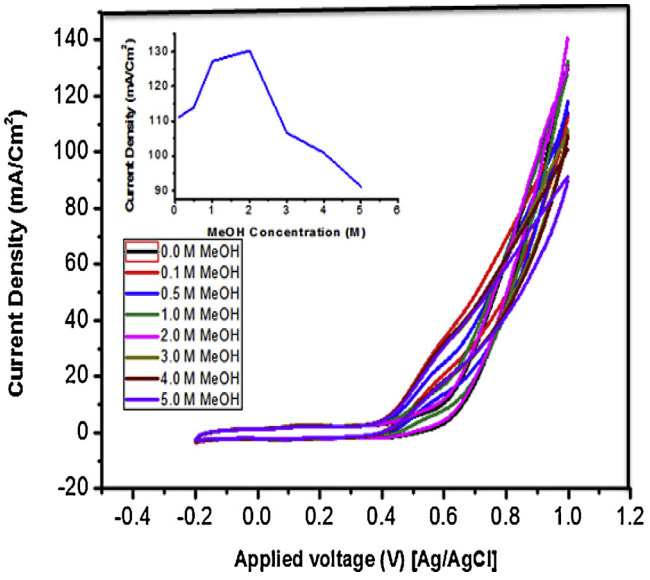

Fig. 12. Cyclic voltammograms of the N (4%)–Co/CNFs at a scan rate of 50 mV s^{-1}, 25 °C, and 1 M KOH at different concentration of methanol.

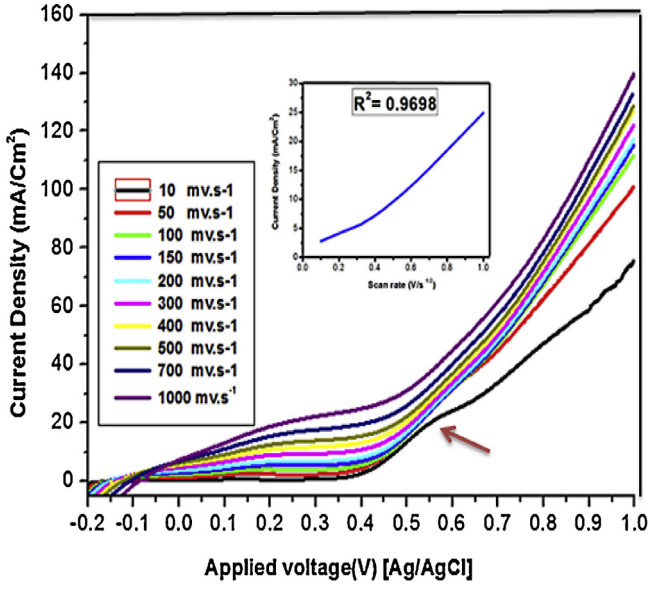

Fig. 13. The linear sweep curves for methanol oxidation on N (4%)–Co/CNFs at different scan rate in 1.0 M KOH containing 3.0 M methanol at 25 °C.

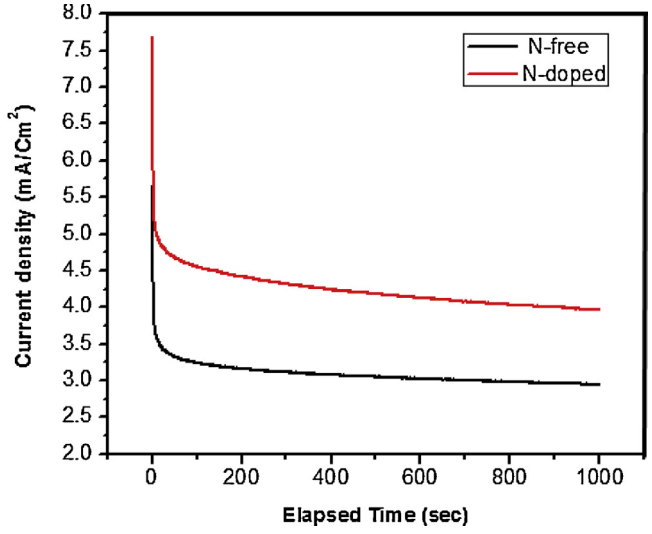

Fig. 14. Chronoamperometric measurement of the Co/N-CNFs (4%) in 1.0 M KOH containing 3.0 M CH_3OH at 0.4 V.

oxidation. It is noteworthy mentioning that the potential peak does not appear at the high scan rates (>50 mV s^{-1}) which means CO is not existent and/or the reaction occurs beyond the applied voltage range [21]. Additionally, the oxidation of the methanol increase with increase the potential scan rate that indicated the electrocatalytic oxidation of methanol on N (4%)–Co/CNFs is controlled by a diffusion process.

3.2.4. Electrode stability

The stability of the non-precious metals electrocatalyst is an important factor for the development anode of DMFCs and might be a new trend in the fuel cells technology. Fig. 14 displays the chronoamperogram of the electroactivity of the N-free and N-doped (4%)Co/CNFs electrodes at an oxidation potential 0.4 V vs. Ag/AgCl in methanol electrooxidation in the 1.0 M KOH and 3.0 M methanol aqueous solution at room temperature. It can be seen from the figure the current density sharply decreases first, and then decreased slowly with increasing the time. The initial decay of current density may due to the formation of intermediate carbonaceous species such as CO_{ads} and CHO_{ads}. As shown in Fig. 14, nitrogen doping did not affect the stability of the introduced nanofibers as both N-free and N-doped Co/C NFs reveal good stability. It is noteworthy mentioning that the steady current density of the N-doped Co/CNFs after 1000 s remained 3.96 mA cm^{-2} which was better than the N-free Co/CNFs (2.94 mA C m^{-2}). It is noteworthy mentioning that the observed good stability can be attributed to sheathing of the metallic nanoparticles by a graphite shell as shown in TEM image (Fig. 8).

4. Conclusion

Cobalt nanoparticles-incorporated nitrogen-doped carbon nanofibers can be synthesized by facile, simple, high yield, low cost, and effective technique; electrospinning. The incorporation of nitrogen in the carbon nanofibers by adding urea to precursor lead to specific anchoring sites for Co NPs along the longitudinal axis after calcination process. The introduced Co/N-CNFs reveal good electrocatalytic activity toward methanol oxidation in alkaline medium due to the influence of the electronic structure of nitrogen that enhances the electronic properties of the carbon nanofibers. Moreover, Co/N-CNFs show good stability toward methanol oxidation for long time. This work is anticipated to open a new possibility to rely on cobalt/N-CNFs as an effective non-precious electrocatalyst for oxidation of small organic compounds.

Acknowledgement

This project was supported by NSTIP strategic technologies programs, number (11-ENE 1917-02) in the Kingdom of Saudi Arabia

References

[1] R. Othman, A.L. Dicks, Z. Zhu, Int. J. Hydrogen Energy 37 (2012) 357–372.
[2] N.V. Long, C.M. Thi, Y. Yong, M. Nogami, M. Ohtaki, J. Nanosci. Nanotechnol. 13 (2013) 4799–4824.
[3] H. An, L. Pan, H. Cui, B. Li, D. Zhou, J. Zhai, Q. Li, Electrochim. Acta 102 (2013) 79–87.
[4] N.V. Long, Y. Yang, C. Minh Thi, N.V. Minh, Y. Cao, M. Nogami, Nano Energy 2 (2013) 636–676.
[5] N.A. Barakat, M.A. Abdelkareem, H.Y. Kim, Appl. Catal. A 455 (2013) 193–198.
[6] N. Hampson, M. Willars, B. McNicol, J. Power Sources 4 (1979) 191–201.
[7] H.A. Gasteiger, N. Markovic, P.N. Ross Jr., E.J. Cairns, J. Phys. Chem. 97 (1993) 12020–12029.
[8] C. Wang, M. Waje, X. Wang, J.M. Tang, R.C. Haddon, Y. Yan, Nano Lett. 4 (2004) 345–348.
[9] W. Li, C. Liang, J. Qiu, W. Zhou, H. Han, Z. Wei, G. Sun, Q. Xin, Carbon 40 (2002) 787–790.
[10] W. Li, C. Liang, W. Zhou, J. Qiu, Z. Zhou, G. Sun, Q. Xin, J. Phys. Chem. B 107 (2003) 6292–6299.
[11] E.S. Steigerwalt, G.A. Deluga, D.E. Cliffel, C. Lukehart, J. Phys. Chem. B 105 (2001) 8097–8101.
[12] Y. Lu, R.G. Reddy, Int. J. Hydrogen Energy 33 (2008) 3930–3937.
[13] N.A. Barakat, M. El-Newehy, S.S. Al-Deyab, H.Y. Kim, Nanoscale Res. Lett. 9 (2014) 1–10.
[14] M.M. Anwar, F.A. Sheikh, H. Kim, Energy Environ. Focus 2 (2013) 171–175.
[15] A. Döner, E. Telli, G. Kardaş, J. Power Sources 205 (2012) 71–79.
[16] N.A. Barakat, M. Abadir, M. Shaheer Akhtar, M. El-Newehy, Y.-s. Shin, H. Yong Kim, Mater. Lett. 85 (2012) 120–123.
[17] N.A. Barakat, M. Motlak, Appl. Catal. B 154 (2014) 221–231.
[18] N.A. Barakat, M. Motlak, B.H. Lim, M.H. El-Newehy, S.S. Al-Deyab, J. Electrochem. Soc. 161 (2014) F1194–F1201.
[19] U. Paulus, A. Wokaun, G. Scherer, T. Schmidt, V. Stamenkovic, V. Radmilovic, N. Markovic, P. Ross, J. Phys. Chem. B 106 (2002) 4181–4191.
[20] S. Zafeiratos, T. Dintzer, D. Teschner, R. Blume, M. Hävecker, A. Knop-Gericke, R. Schlögl, J. Catal. 269 (2010) 309–317.
[21] N.A. Barakat, M.A. Abdelkareem, A. Yousef, S.S. Al-Deyab, M. El-Newehy, H.Y. Kim, Int. J. Hydrogen Energy 38 (2013) 3387–3394.
[22] N.A. Barakat, M.A. Abdelkareem, M. El-Newehy, H.Y. Kim, Nanoscale Res. Lett. 8 (2013) 1–6.
[23] F.A. Sheikh, J. Macossay, M.A. Kanjwal, A. Abdal-hay, M.A. Tantry, H. Kim, Int. Sch. Res. Not. 2012 (2012) 1–10.
[24] X. Xu, Y. Zhou, T. Yuan, Y. Li, Electrochim. Acta 112 (2013) 587–595.
[25] B. Vinayan, K. Sethupathi, S. Ramaprabhu, Int. J. Hydrogen Energy 38 (2013) 2240–2250.

[26] Y. Xin, J.-g. Liu, X. Jie, W. Liu, F. Liu, Y. Yin, J. Gu, Z. Zou, Electrochim. Acta 60 (2012) 354–358.
[27] Y. Shao, G. Yin, Y. Gao, P. Shi, J. Electrochem. Soc. 153 (2006) A1093–A1097.
[28] S. Maldonado, K.J. Stevenson, J. Phys. Chem. B 109 (2005) 4707–4716.
[29] S. Dommele, K.P. áde Jong, Chem. Commun. (2006) 4859–4861.
[30] Y. Shao, J. Sui, G. Yin, Y. Gao, Appl. Catal. B 79 (2008) 89–99.
[31] R.A. Sidik, A.B. Anderson, N.P. Subramanian, S.P. Kumaraguru, B.N. Popov, J. Phys. Chem. B 110 (2006) 1787–1793.
[32] R. Liu, D. Wu, X. Feng, K. Müllen, Angew. Chem. 122 (2010) 2619–2623.
[33] H. Yoon, S. Ko, J. Jang, Chem. Commun. (2007) 1468–1470.
[34] B.M. Thamer, M.H. El-Newehy, N.A. Barakat, M.A. Abdelkareem, S.S. Al-Deyab, H.Y. Kim, Electrochim. Acta 142 (2014) 228–239.
[35] N.A. Barakat, M.A. Kanjwal, F.A. Sheikh, H.Y. Kim, Polymer 50 (2009) 4389–4396.
[36] N.A. Barakat, M.S. Khil, F.A. Sheikh, H.Y. Kim, J. Phys. Chem. C 112 (2008) 12225–12233.
[37] N.A. Barakat, K.-D. Woo, S. Ansari, J.-A. Ko, M.A. Kanjwal, H.Y. Kim, Appl. Phys. A: Mater. Sci. Process. 95 (2009) 769–776.
[38] N.A.M. Barakat, M.F. Abadir, F.A. Sheikh, M.A. Kanjwal, S.J. Park, H.Y. Kim, Chem. Eng. J. 156 (2010) 487–495.
[39] N.A. Barakat, K.A. Khalil, I.H. Mahmoud, M.A. Kanjwal, F.A. Sheikh, H.Y. Kim, J. Phys. Chem. C 114 (2010) 15589–15593.
[40] N.A. Barakat, B. Kim, S. Park, Y. Jo, M.-H. Jung, H.Y. Kim, J. Mater. Chem. 19 (2009) 7371–7378.
[41] C.F. Chang, Q.D. Truong, J.R. Chen, Appl. Surf. Sci. 264 (2013) 329–334.
[42] İ. Uslu, F. Gökmeşe, O. Atakol, M.L. Aksu, Hacettepe J. Biol. Chem. 37 (2009) 227–231.
[43] Z.R. Ismagilov, A.E. Shalagina, O.Y. Podyacheva, A.V. Ischenko, L.S. Kibis, A.I. Boronin, Y.A. Chesalov, D.I. Kochubey, A.I. Romanenko, O.B. Anikeeva, Carbon 47 (2009) 1922–1929.
[44] N.A.M. Barakat, K.A. Khalil, I.H. Mahmoud, M.A. Kanjwal, F.A. Sheikh, H.Y. Kim, J. Phys. Chem. C 114 (2010) 15589–15593.
[45] N.A.M. Barakat, B. Kim, S.J. Park, Y. Jo, M.-H. Jung, H.Y. Kim, J. Mater. Chem. 19 (2009) 7371–7378.
[46] A. Yousef, N.A.M. Barakat, T. Amna, A.R. Unnithan, S.S. Al-Deyab, H. Yong Kim, J. Lumin. 132 (2012) 1668–1677.
[47] N.A.M. Barakat, M.F. Abadir, M. Shaheer Akhtar, M. El-Newehy, S. Y-s, H. Yong Kim, Mater. Lett. 85 (2012) 120–123.
[48] N.A.M. Barakat, A.G. El-Deen, G. Shin, M. Park, H.Y. Kim, Mater. Lett. 99 (2013) 168–171.
[49] N.A.M. Barakat, M. Motlak, Appl. Catal. B 154–155 (2014) 221–231.
[50] A. Shukla, P. Christensen, A. Hamnett, M. Hogarth, J. Power Sources 55 (1995) 87–91.
[51] H.N. Dinh, X. Ren, F.H. Garzon, P. Zelenay, S. Gottesfeld, J. Electroanal. Chem. 491 (2000) 222–233.
[52] A. Hamnett, Catal. Today 38 (1997) 445–457.
[53] S. Mahapatra, J. Datta, Int. J. Electrochem. 2011 (2011) 1–16.